https://dx.doi.org/10.1016/j.apenergy.2021.117012

Optimization of catalyst layer thickness for achieving high performance and low cost of high temperature proton exchange membrane fuel cell

Lingchao Xia [a], Meng Ni [a, *], Qidong Xu [a], Haoran Xu [a,b], Keqing Zheng [c,*]

[a] *Building Energy Research Group, Department of Building and Real Estate, The Hong Kong Polytechnic University, Hung Hom, Kowloon, Hong Kong, China*

[b] *Department of Chemical Engineering, Loughborough University, Loughborough, United Kingdom*

[c] *School of Electrical and Power Engineering, China University of Mining and Technology, Xuzhou, China*

Corresponding authors:

Email: meng.ni@polyu.edu.hk (M.Ni); keqingzheng@126.com (K.Q. Zheng)

Abstract: The thickness of catalyst layer (CL) determines the electrochemical performance and the cost of high temperature proton exchange membrane fuel cell (HT-PEMFC). However, various values (e.g. 100 μm, 50 μm, 10 μm) of CL thickness are reported in the previous studies. To identify the optimal CL thickness to reduce the PEMFC cost without sacrificing the electrochemical performance, it is necessary to first identify the effective reaction thickness (ERT) of both anode and cathode. A numerical non-isothermal 3D model was developed considering the activation loss, concentration loss and ohmic loss at two electrodes, respectively. After model validation, parametric analyses were performed to investigate the effects of temperature, working voltage and flow rate on the performance of the fuel cell, especially on ERT. It is found that the ERT increases with increasing temperature. The working voltage and the cathode flow rate have opposite influences on the ERT of the two electrodes. The ERT highly depends on the ratio of activation loss and concentration loss ($\eta_{act+}\eta_{conc}$) to ohmic loss η_{ohmic}.

Considering the utilization rate of the catalyst and cell performance, the appropriate CL thicknesses for anode and cathode electrode are 10-17 μm and 15-30 μm, respectively. This study clearly demonstrates that we can reduce the CL cost and maintain high fuel cell performance by carefully controlling the thickness of CL.

Key words: HT-PEMFC; Active reaction thickness; Potential loss ratio; Effective reaction area.

Nomenclature

E	Ideal voltage [V]	η_{ohmic}	Ohmic loss [V]
E^0	Open circuit voltage [V]	η_{conc}	Concentration loss [V]
E_a	Activation energy [J/mol]	η_{act}	Activation loss [V]
T	Operating temperature [°C]	R_{ohmic}	Ohmic resistance [ohm]
$a_{pro}^{v_i}$	Product pressure [Pa]	R_{elec}	Electron resistance [ohm]
$a_{rea}^{v_i}$	Reactant pressure [Pa]	R_{ionic}	Ionic resistance [ohm]
R	Universal gas constant [J/mol/K]	n	Moles [mol]
F	Faraday constant [C/mol]	c_R^0	Reactant concentration in GDL [mol/m^3]
j_0	Exchange current density [A/cm^2]	c_R^*	Reactant concentration in CL [mol/m^3]
j	Current density [A/cm^2]	α	Charge transfer coefficient
i	Current [A]	DL	Doping level of H_3PO_4
u	Velocity [m/s]	ρ	Density [kg/m^3]
Q	Heat generation [J]	μ	Dynamic viscosity [kg/m·s]
k	Thermal conductivity [W/m·K]	C_p	Heat capacity [J/mol·K]

PtC	Platinum to carbon ratio	R_{pt}	Surface area per unit mass [m^2/g]

1. Introduction

Proton exchange membrane fuel cells (PEMFCs) are considered as one of the most promising power generation devices to replace conventional power sources. High temperature proton exchange membrane fuel cells (HT-PEMFCs) working at 120 to 200 °C can avoid water flooding phenomenon [1, 2] in the low temperature PEMFC (LT-PEMFC). Besides simplified water management [3], higher working temperature also brings the advantages of higher CO tolerance [4], and elevated reaction kinetics [5, 6]. A lot of works related to HT-PEMFC were reported in the last decade. Most of them focused on the flow field design [7-10], material development [11-13], degradation analysis [14-16] and system optimization [17-20]. However, the commercialization of HT-PEMFC is still hindered by some challenges. It is reported by U.S. Department of Energy that although HT-PEMFC shows a better cell performance, its stack cost (US\$840 kW^{-1}) is 47% higher than that of low temperature stack at low production volumes [21]. Since the platinum catalyst used in the catalyst layer (CL) accounts for a large proportion of the total cost, it is expected that the fuel cell cost can be reduced by reducing the catalyst loading or reducing the thickness of CL without sacrificing the cell performance.

The advantages of HT-PEMFC mentioned above provide the opportunity of using low Pt loading or even Pt free catalysts [22, 23], which can reduce the cost of catalyst. However, the cell performance with non-Pt catalysts is still not good enough [24], which makes the research of Pt based catalyst necessary. Bevilacqua et al. [25] recently

reported better cell performance with Pt_3Co/C catalyst due to its larger average pore size of Pt_3Co compared with that of pure Pt. Eirini et al. [26] reported lower cell performance with a higher thickness of H_3PO_4/H_2O in CL because of the lower diffusion rate of reactants. Martin et al. [27] prepared an ultra-low Pt loading of ~0.1 $mg_{Pt}cm^{-2}$ at cathode and a peak power density of 321 $mWcm^{-2}$ was obtained with a specific Pt utilization of 1.7 kWg_{Pt}^{-1}. A higher peak power density of 346 $mWcm^{-2}$ [28] was achieved when reducing the anodic Pt loading to 0.5 $mg_{Pt}cm^{-2}$ in their next study. However, whether the cell performance with other Pt loadings could be higher or not requires further investigation. It is needed to conduct a research with a wider range of Pt loading and CL thickness to reveal the relationship between them and cell performance. The CFD-based models should be used for this purpose as these models can obtain detailed data and help understand complicated processes inside the fuel cell.

By now, the simulation works conducted on the CL are limited. Models with different scales such as nano-/micro-scale model [29] and macro-scale [30, 31] model have been established before to better understand the porous electrocatalyst layer. When it comes to the single cell modelling, the research focus diverts to the parametric design. Scott et al. [32] developed an isothermal one-dimensional model of HT-PEMFC to study the effect of catalyst loading and Pt/carbon ratio, and reported that the peak power density can be acquired with a 40 wt.% Pt/C ratio. However, Krerkkiat et al. [33] reported that a higher ratio of ionomer/Pt/C would lead to agglomeration of catalyst particle and a decrease of cell performance. Based on Scott's work [32], Kamarajugadda et al. [34] developed a two-dimensional model to investigate the effect

of cathode catalyst layer's structure. In this model, the polarization curves with different cathode thicknesses were achieved and an optimum value of 60 nm of polymer coating thickness was suggested. A three dimensional isothermal model by Zhang et al. [35] is developed with the catalyst layers to be 10 μm, 20 μm, 30 μm, 50 μm and 100 μm. The polarization curves show that a better cell performance can be achieved by reducing the thickness of CL. However, two CL thicknesses were changed together while the effect of anode and cathodic CL thicknesses might be different. In fact, a low catalyst loading for anode CL is enough due to easier hydrogen oxidation reaction (HOR) [24]. More importantly, the previous study [35] neglected the effect of CL thickness on activation loss of the fuel cell. since only the effects of CL thickness on electron/ion conduction and gas transport were considered, the conclusion that the fuel cell performance could be continuously improved by reducing the CL thickness could be incorrect and should be re-evaluated.

As the electrochemical reaction takes place in the CL, the thickness of CL could significantly influence the performance of HT-PEMFC. Thus, the CL thickness must be carefully designed to reduce the cost and to achieve high fuel cell performance. In order not to sacrifice the performance while minimizing the CL thickness, the first step is to identify the effective reaction thickness (ERT). Based on the literature review, although some studies have been performed on the electrochemical reaction distributions in the CL of high temperature solid oxide fuel cells (SOFCs), no relevant study has been conducted for HT-PEMFC. In practice, the CL thickness is about 50μm. It is expected that the CL cost can be decreased by simply reducing the CL thickness. Can we still

maintain good performance while we reduce the CL thickness? What is the minimum CL thickness to provide the required reaction sites for the electrochemical reactions in HT-PEMFC? In order to answer these scientific questions, an in-depth understanding on the reaction distribution in the CL and a detailed analysis and optimization of the ERT of HT-PEMFC are needed.

For the study of HT-PEMFC, the low-cost, high performance and splendid durability are the three key objectives [36]. This work tries to provide a solution to the former two goals of low-cost and high performance. In this work, a numerical non-isothermal 3D model was developed to investigate the ERT of both anode and cathode catalyst layer of HT-PEMFC. For the first time, the potential losses including the activation loss, concentration loss and ohmic loss in HT-PEMFC were calculated respectively at the two electrodes with full consideration of the coupled transport and reaction in the CL. The comparison between economic cost and cell performance was performed to determine the most appropriate values of CL thickness.

The new contributions of this work include: (1) identifying CL thickness to achieve high performance with minimal catalyst cost; (2) defining and calculating effective reaction thickness (ERT) which shows the level of reaction's aggregation. The method of determining the appropriate CL thickness adopted in this work can be further applied to other types of fuel cells.

2. Model development

2.1 Computational domain and assumptions

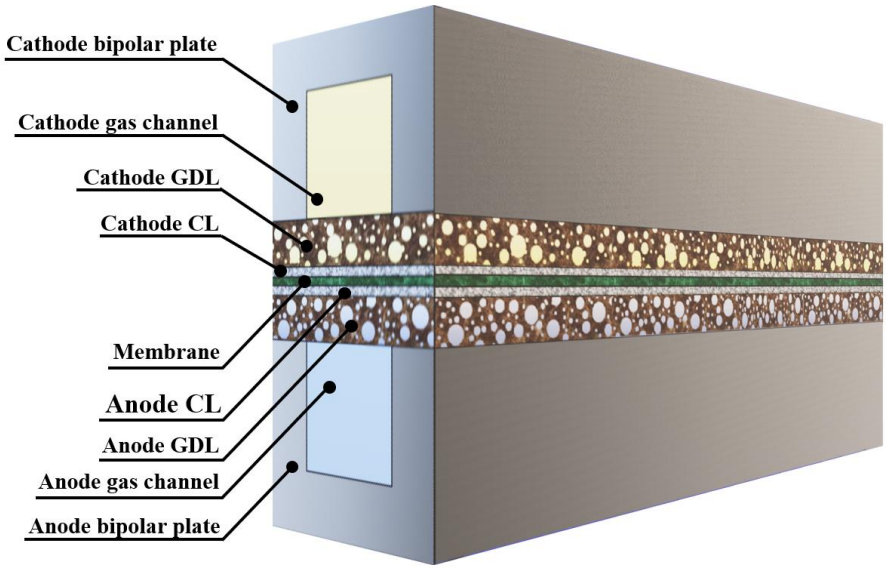

Fig. 1. Schematic of computational domain

The computational domain of HT-PEMFC is composed of 9 main parts including two bipolar plates (BP), two gas channels, two gas diffusion layers (GDL), two catalyst layers (CL) and one proton exchange membrane as shown in Fig .1. Main assumptions are as follows: (1) Fully developed laminar flow in gas channel; (2) Impermeable membrane to all reactants; (3) Isotropic and homogenous porous media of GDL and CL; (4) Steady-state operation of HT-PEMFC; (5) Uniformly distributed catalyst in the CL.

2.2 Governing equations

2.2.1 Electrochemistry

In this model, oxygen reduction reaction (ORR) and hydrogen oxidation reaction (HOR) take place in the cathode and anode, respectively.

Anode:

$$H_2 \rightleftharpoons 2H^+ + 2e^- \tag{1}$$

Cathode:

$$\frac{1}{2}O_2 + 2H^+ + 2e^- \rightleftharpoons H_2O \quad (2)$$

Both reactions at two CLs are described using the Butler-Volmer equations.

$$i_a = i_{0,a}\left(\frac{C_{H_2}}{C_{H_{2,ref}}}\right)^{0.5}\left(e^{\frac{n\alpha_a F}{RT}\eta_a} - e^{\frac{-n(1-\alpha_a)F}{RT}\eta_a}\right) \quad (3)$$

$$i_c = i_{0,c}\left(\frac{C_{O_2}}{C_{O_{2,ref}}}\right)^{1}\left(-e^{\frac{n(1-\alpha_c)F}{RT}\eta_c} + e^{\frac{-n\alpha_c F}{RT}\eta_c}\right) \quad (4)$$

where η_a and η_c represent the activation losses at the two electrodes and can be calculated by:

$$\eta_a = \phi_s^a - \phi_l^a - E_{eq}^a \quad (5)$$

$$\eta_c = \phi_s^c - \phi_l^c - E_{eq}^c \quad (6)$$

where ϕ represents the electric potential and E_{eq} represents the equilibrium electric potential. In this work, E_{eq} at the two electrodes are set as:

$$E_{eq}^a = 0; \quad E_{eq}^c = E_{Nernst} \quad (7)$$

Membrane conductivity is dependent on the local temperature and doping level of phosphoric acid which can be calculated by:

$$\sigma_{\text{mem}} = \sigma_0 \exp\left[\frac{-619.6DL+21750}{R}(-1/T + 1/453.15)\right] \quad (8)$$

where σ_0 represents the electrolyte conductivity at 180 °C and *DL* is set as 5 according to the reference [37]. The typical microstructure properties such as the permeability and the porosity of the CL are used in the present study. In the fabrication of the CL, the use of ionomer is critical as the ionomer content can influence the Pt loading, the permeability and porosity of the CL. Thus, the microstructure properties of the CL can be adjusted by controlling the ionomer carbon ratio (I/C ratio). For example, in ref. [38], the I/C ratio effect on fuel cell performance was studied and an optimal I/C

ratio of 1.0 was found. In other studies, the effects of I/C ratio on the gas transport properties have also been studied. In this study, the typical permeability and porosity of the CL resulting from the typical I/C ratio were used. In the CL, the transport of the ions and electrons can be described by ohm's law. As the catalyst layer is porous, the effective conductivity should be modified with due consideration of the porosity effect, as shown as the Bruggeman equation:

$$\sigma_{l,\mathrm{CL}} = \varepsilon^{1.5}\sigma_l \tag{9}$$

where ε represents the porosity. The pores inside the catalyst layer also affects the mass transport. Thus, the diffusion coefficient should consider the porosity effect and determined by equation:

$$D_{\mathrm{eff}} = \frac{\varepsilon}{\tau} D_0 \quad , \quad \tau = \varepsilon^{-1/2} \tag{10}$$

The exchange current density is calculated by:

$$i_{0,a/c} = A_{\mathrm{v}} \bullet i_{0,a/c\_ref} \tag{11}$$

where A_{v} is catalyst layer's specific surface area, i_{0,a_ref} and i_{0,c_ref} are reference exchange current density at anode and cathode catalyst layer, respectively. The values are governed by temperature dependent equation [39]:

$$i_{0,a\_ref} = 7.135\exp[-1400(1/T - 1/353.15)] \tag{12}$$

$$i_{0,c\_ref} = 1.2286\text{e-}6\exp[-7900(1/T - 1/353.15)] \tag{13}$$

The specific surface area of catalyst layer A_{v} is determined by:

$$A_{\mathrm{v}} = \frac{A_{act}}{V_{a/c}} \tag{14}$$

where A_{act} is catalyst particles' active area and $V_{\mathrm{a/c}}$ is catalyst layer's volume. The active

area A_{act} is governed by [32]:

$$A_{act} = Ld \bullet ab \bullet R_{pt} \tag{15}$$

where Ld represents loading level of Pt catalyst, a and b are the length and width of the cell, R_{pt} is catalyst surface per unit mass determined by the polynomial fitting function according to the Table 1:

$$R_{pt} = 32.5839PtC^3 + 87.5837PtC^2 - 286.1994PtC + 166.8393 \tag{16}$$

where PtC represents platinum to carbon ratio.

Table.1 Catalyst platinum surface area per unit mass under different platinum to carbon ratio [40]

Platinum to carbon ratio, PtC	Surface area per unit mass, R_{pt} (m^2/g)
10%	140
20%	112
30%	88
40%	72
60%	32
80%	11
100%	28

2.2.2 Flow field and mass transport

Navier-Stokes equation is used to model the momentum transfer of the laminar gas flow in channels.

$$\rho(\frac{\partial \vec{v}}{\partial t} + \vec{v} \bullet \nabla \vec{v}) = \nabla \left\{ -P\vec{I} + \mu[\nabla \vec{v} + (\nabla \vec{v})^T] \right\} \tag{17}$$

Mass transport is governed by:

$$\nabla\left\{-\rho w_i\sum_{j=1}^{N}D_{ij}[\frac{M}{M_j}\left(\nabla w_j+w_j\frac{\nabla M}{M}\right)+\left(x_j-w_j\right)\frac{\nabla P}{P}]+w_i\rho\vec{v}\right\}=R_i \quad (18)$$

The molar fraction of nitrogen in the cathode can be obtained as:

$$w_{N_2}=1-w_{O_2}-w_{H_2O} \quad (19)$$

The gas velocity is based on the stoichiometric (St) number, molar fraction, and temperature by:

$$U_{in\_\ cathode}=\lambda_c\frac{I}{4F}w_{O_2}RT/(P\bullet A_{channel}) \quad (20)$$

$$U_{in\_anode}=\lambda_a\frac{I}{2F}w_{H_2}RT/(P\bullet A_{channel}) \quad (21)$$

Table 2 lists the dynamic viscosities of each specie which are temperature dependent. The dynamic viscosity and density of gas mixture can be obtained by:

$$\mu_{a,c}=\sum_{i=1}^{n}\frac{w_i\mu_i}{\sum_{j=1}^{n}(w_j\sqrt{\frac{M_j}{M_i}})} \quad (22)$$

$$\rho=\mathrm{p}(\mathrm{RT}\sum_i\frac{w_i}{M_i})^{-1} \quad (23)$$

Table 2 Thermal properties [41]

Parameters	Value
Dynamic viscosity of H_2	(27.758+2.12E-1*T-3.28E-5*T*T) *1e-7 [Pa·s]
Dynamic viscosity of N_2	(42.606+4.75E-1*T-9.88E-5*T*T) *1e-7 [Pa·s]
Dynamic viscosity of O_2	(44.224+5.62E-1*T-1.13E-5*T*T) *1e-7 [Pa·s]
Dynamic viscosity of H_2O	(-36.826+4.29E-1*T-1.62E-5*T*T) *1e-7 [Pa·s]
Heat capacities of H_2	25.40+2.0178E-2*T-3.8549E-5*T^2+3.1880E-8*T^3-8.7585E-12*T^4 [J/mol·K]
Heat capacities of N_2	29.34-3.5395E-3*T+1.0076E-5*T^2-4.3116E-9*T^3+2.5935E-13*T^4 [J/mol·K]
Heat capacities of O_2	29.53-8.8999E-3*T+3.8083E-5*T^2-3.2629E-

Heat capacities of H_2 O	8*T^3+8.8607E-12*T^4 [J/mol·K]
	33.93-8.4186E-3*T+2.9906E-5*T^2-1.7825E-8*T^3+3.6934E-12*T^4 [J/mol·K]
Thermal conductivities of H_2	0.03591+4.5918E-4*T-6.4933E-8*T^2 [W/m/K]
Thermal conductivities of N_2	0.00309+7.5930E-5*T-1.1014E-8*T^2 [W/m/K]
Thermal conductivities of O_2	0.00121+8.6157E-5*T-1.3346E-8*T^2 [W/m/K]
Thermal conductivities of H_2O	0.00053+4.7093E-5*T+4.9551E-8*T^2 [W/m/K]

2.2.3 Heat transfer

Heat generation by two half-reactions at two catalyst layers can be calculated by:

$$Q_{\text{react\_a/c}} = (-T\Delta S_{a/c}) \cdot \frac{I}{nF} \tag{24}$$

where ΔS_a and ΔS_c represent the entropy change of anode and cathode, respectively. The absolute entropy of each specie is listed in Table 3. Thus, ΔS can be calculated by:

$$\Delta S_a = 2S°[H^+(g)] + 2S°[e^-(g)] - S°[H_2(g)] \tag{25}$$

$$\Delta S_c = S°[H_2O(g)] - 2S°[e^-(g)] - 2S°[2H^+(g)] - \frac{1}{2}S°[O_2(g)] \tag{26}$$

Heat generation by ohmic loss and activation loss can be calculated by:

$$Q_{\text{oh}} = \eta_{ohmic} \cdot I \cdot A_{\text{react}} \tag{27}$$

$$Q_{\text{act\_a/c}} = j_{a/c} \, | \eta_{act\_a/c} | \tag{28}$$

Thus, the total heat generation can be determined as:

$$Q_{\text{total}} = Q_{\text{react}} + Q_{\text{oh}} + Q_{\text{act}} \tag{29}$$

Energy equation is adopted for heat transfer by:

$$\nabla \cdot (\rho C_p \vec{v} T) = \nabla \cdot (k \nabla T) + S_T \tag{30}$$

where thermal conductivity k and heat capacity C_p of gas mixtures are dependent on mass fraction Y_i of each specie by:

$$C_{\mathrm{p}} = \sum_i w_i (C_{\mathrm{p}})_i \tag{31}$$

$$k = \sum_i Y_i k_i \tag{32}$$

Table 3 Absolute entropy of each specie [42]

Temperature [K]	H_2 [J·K^{-1}·mol^{-1}]	O_2 [J·K^{-1}·mol^{-1}]	H^+ [J·K^{-1}·mol^{-1}]	e^- [J·K^{-1}·mol^{-1}]	H_2O [J·K^{-1}·mol^{-1}]
298.15	130.68	205.157	108.946	20.979	188.834
300	130.858	205.329	109.075	21.107	189.042
350	135.315	209.88	112.279	24.311	/
400	139.216	213.871	115.055	27.087	198.788
450	142.656	217.445	117.503	29.535	/
500	145.737	220.693	119.693	31.725	206.634

Table 4 Physical/chemical properties and operating conditions [43]

Parameters	Value
Channel length	20 [mm]
Channel height	1 [mm]
Channel width	0.7874 [mm]
Rib height	1 [mm]
Rib width	0.9093 [mm]
GDL thickness	0.38 [mm]
CL thickness	0.05 [mm]
Membrane thickness	0.1 [mm]
Collector thickness	0.5 [mm]
Humidified temperature, T_H	28 [°C]
Working temperature, T_w	180 [°C]
GDL porosity, ε_{GDL}	0.4
GDL permeability, K_{GDL}	1.18e-12 [m^2]
CL porosity, ε_{CL}	0.4
Cl permeability, K_{CL}	K_{GDL} /5 [m^2]
Anode stoichiometry number, λ_a	1.2
Cathode stoichiometry number, λ_c	2.0
Molar fraction of H_2, w_{H2}	0.963
Molar fraction of H_2O, w_{H2O}	0.037
Molar fraction of O_2, w_{O2}	0.202
Molar fraction of N_2, w_{N2}	1- w_{O2} -w_{H2O}
Molar mass of H_2, M_{H2}	2 [g/mol]
Molar mass of N_2, M_{N2}	28 [g/mol]
Molar mass of H_2O, M_{H2O}	18 [g/mol]
Molar mass of O_2, M_{O2}	32 [g/mol]

Anode charge transfer coefficient, α_a	0.5
Cathode charge transfer coefficient, α_c	0.25
Electrolyte conductivity at 180°C, σ_0	9.825 [S/m]
Electrode conductivity, σ_s	222 [S/m]
Bipolar plate conductivity, σ_b	20,000 [S/m]
Reference pressure, P_r	1 [atm]
Ratio of Pt to C, PtC	0.3

2.3 Boundary conditions

The HT-PEMFC works with open-end anode and cathode. Proton exchange membrane is impermeable to all reactants. Back pressures at outlets of both anode and cathode outlets are 1 atm. Hydrogen and air are both humidified with a temperature of 28 °C.

The surface of cathodic BP is as 0 V and working voltage is applied to the surface of anodic BP. No-slip condition is adopted for internal surfaces. The other walls are adiabatic. Only protons can pass through the electrolyte and membrane. Only electron conduction is considered in the GDL while both electron conduction and proton conduction are considered in the CL.

3. Results and analysis

3.1 Model validation

Before model validation, gird independence check was performed at a working voltage of 0.6V, as shown in Fig. 2. It can be seen that the current density decreases significantly when the number of elements increases from 2500 to 20000. Then, it approaches to a constant value with further increase in meshing elements. Another curve shows that the computational time almost linearly increases with increasing

number of meshing elements. Considering the computational time and the accuracy, 74800 elements are adopted in this study.

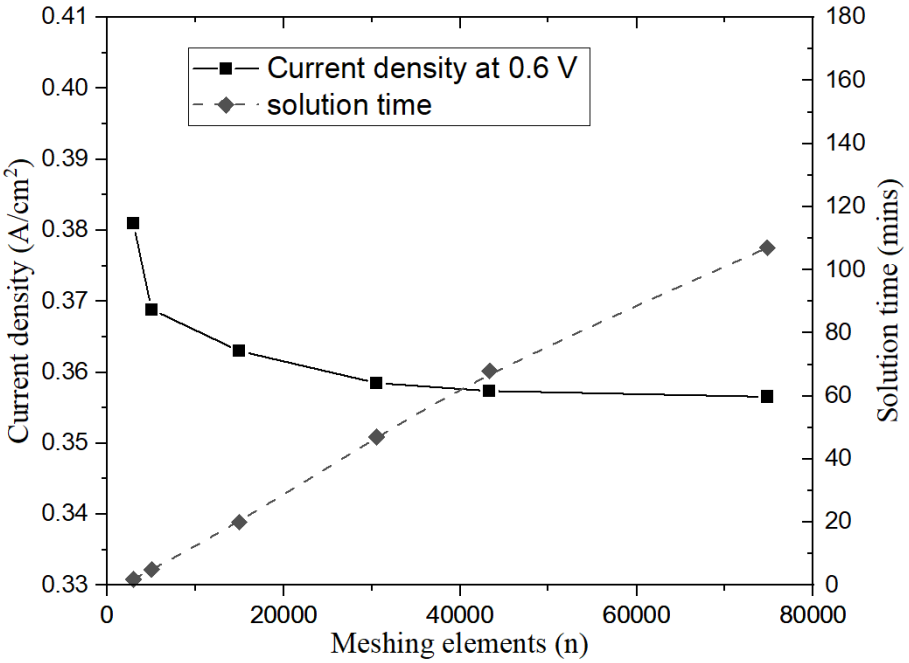

Fig. 2. Grid independence analysis

After gird independence analysis, preliminary simulation was performed and compared with experimental data [43] for model validation as can be seen in Fig. 3. The simulation model shares the same geometric and operating parameters with those in the experiment. The operating temperature is 180 °C. Fuel cell operates with humidified hydrogen and air at atmospheric pressure. Stoichiometry number is 1.2 and 2 for anode and cathode, respectively.

The simulation results show a very good agreement with the experiment values in the low current density region, which implies that the activation loss is well simulated. When the current density is relatively large, the simulation results are slightly lower than the experimental results. This can be attributed to the compression effect during

the assembly process of fuel cell which would lead to a thinner CL and GDL. Therefore, smaller ohmic loss is observed in the experiment due to the smaller distance for ion and electron transportation. Based on the model validation, the simulation model can be adopted for further study.

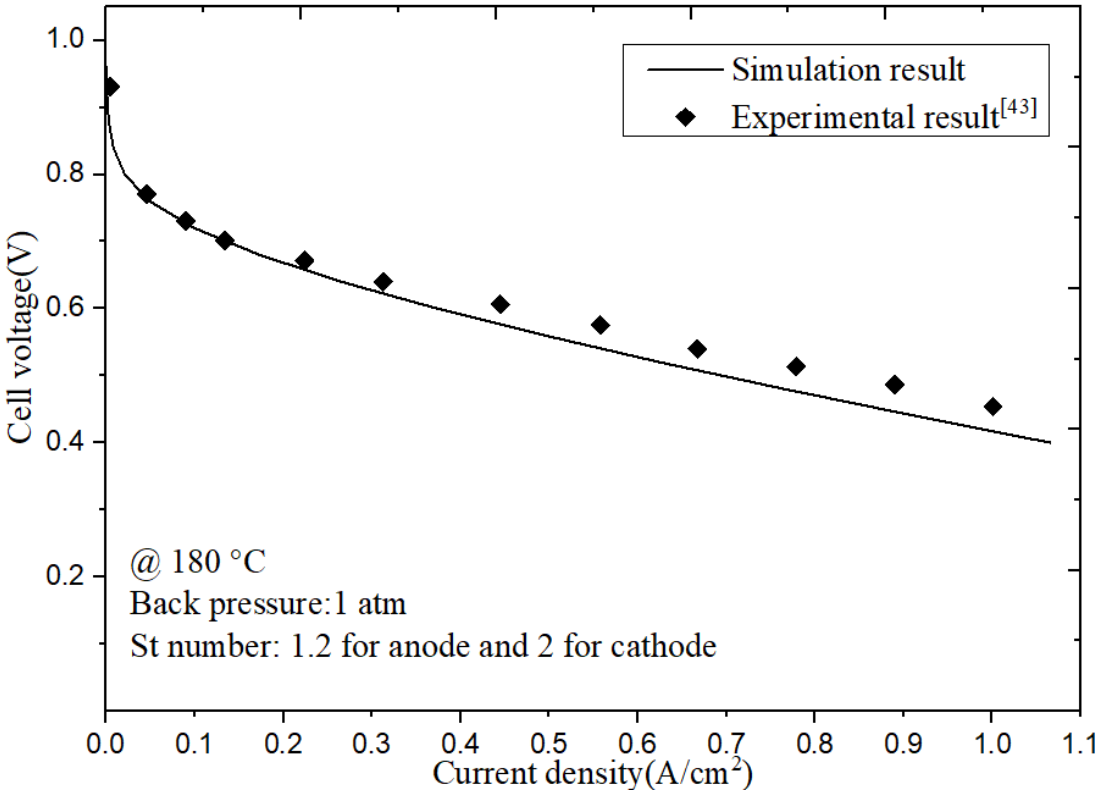

Fig. 3. Simulation results in comparison with experimental data [43]

3.2 Effective reaction thickness

Generally, the parametric simulation study is based on a typical cell configuration as listed in Table 4. In this section, the effective reaction thickness is studied.

3.2.1 Effect of operating conditions

Fig. 4 shows the current density distribution in the CL of anode and cathode. The results with different temperatures are obtained at a voltage of 0.4 V (Fig.4(a)) and the results with different voltages are at a temperature of 160 °C (Fig.4(b)). It is clearly

to see that the current density is the highest at the electrode-electrolyte interface and decreases significantly with increasing distance away from this interface. Such distribution is caused by the low effective ionic conductivity of the CL due to the low volume fraction of the ionic phase in the CL and the tortuous paths for ion transport. Thus, high electrochemical reaction rate occurs at the electrode-electrolyte interface in order to minimize the ohmic loss of ion (proton) transport. It can be seen that the decreasing rate at anode side is much higher than that at cathode side since HOR is much easier than ORR [44] which leads to a more concentrated reaction area at anode.

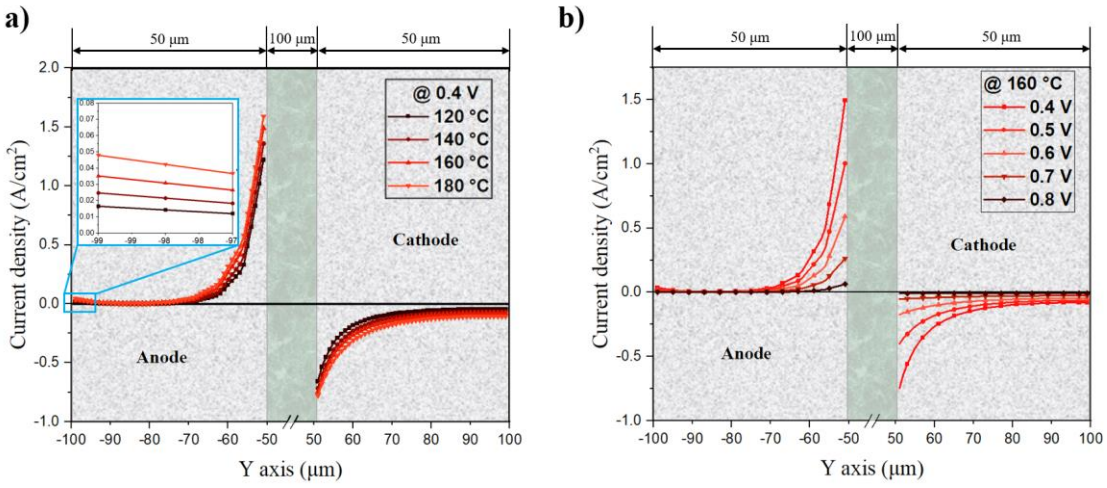

Fig. 4. Current density at various locations at a) different temperatures and b) different voltages

Temperature would affect the electrolyte conductivity and reference current density (see Eq. (8) and Eq. (12)). The increase of temperature would lead to a better cell performance in terms of higher current density in the catalyst layer which can be seen in Fig. 4(a). Similar result was reported by Lai [21]. The working voltage is another parameter influencing the distribution of reaction. Lower voltage leads to a significant increment of the current density next to the membrane compared with that at the

positions away from the membrane.

However, it should be noted that a small current density would occur at the interface between catalyst layer and gas diffusion layer (GDL) in the magnification picture of Fig. 4(a). This phenomenon can be attributed to the high concentration of reactants and relatively low electronic resistance in this region. Similar phenomenon was also reported in solid oxide fuel cell (SOFC) by Chen et. al [45].

3.2.2 Definition of ERT

In this study, the effective reaction thickness (ERT) is defined as the thickness of the CL which covers 95% of the total electrochemical reaction, as shown in Fig. 5(a). 95% is high enough to account for most of the electrochemical reactions. A higher value (99%) may cause high sensitivity of the computed ERT to various parameters. With such a definition, different ERTs of both anode and cathode can be obtained at different voltages (see Fig. 5(b)). After achieving the ERT at different locations along the flow channel, the variation of ERT along the flow direction can be obtained (see Fig. 5(c, d, e & f)). As shown in Fig. 5(c & d), the ERT is found to increase with increasing temperature at 0.4 V. Similarly, the ERT is found to increase along the flow channel at both anode and cathode. However, it can be seen that the temperature effect on anode is much more significant than that on cathode. ERT is increased by around 8 μm at anode while the increment is only 1.2 μm at cathode.

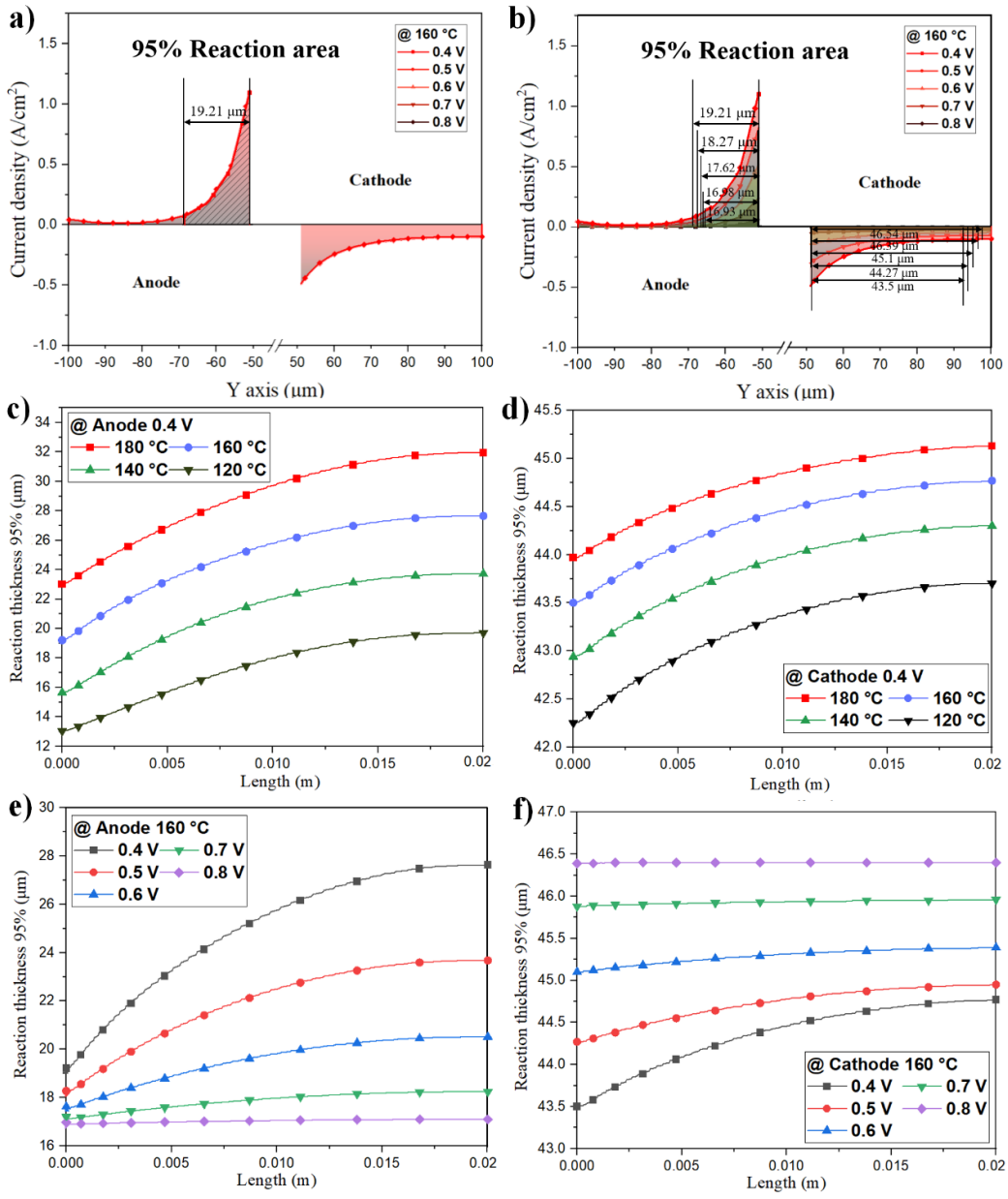

Fig. 5. a) Schematic of effective reaction area, b) Effective reaction thickness at different voltages, Effective reaction thickness of c) anode and d) cathode at different temperatures along the flow direction, Effective reaction thickness of e) anode and f) cathode at different voltages along the flow direction

The effects of working voltage on ERT are opposite for anode and cathode in Fig. 5(e & f). When the voltage decreases from 0.8 V to 0.4 V, ERT is increased at anode but decreased at cathode. At a high voltage, the ERT remains almost unchanged along

the flow channel. At a low voltage, the ERT increases along the flow channels at the anode and cathode.

3.2.3 Potential losses

To gain a fundamental understanding of the phenomenon mentioned above, various potential losses are illustrated in Fig. 6. It has two interfaces including the CL/GDL interface and CL/MEM interface. The CL thickness is 50 μm. Thus, the potential losses for specific location at a given current density consist of: 1) activation loss by the electrochemical process (η_{act}) with the change of Nernst voltage considered caused by variation of reactants concentration, 2) concentration loss by the differential concentration between reaction site and gas channel (η_{conc}), 3) ohmic losses by the electron transportation (R_{el}) between reaction site and current collector and ion transportation (R_{io}) between reaction site and membrane (η_{ohmic}). Since the reaction rate can be significantly affected by the reactants distribution, the η_{act} and η_{conc} can be combined together as $\eta_{act+conc}$.

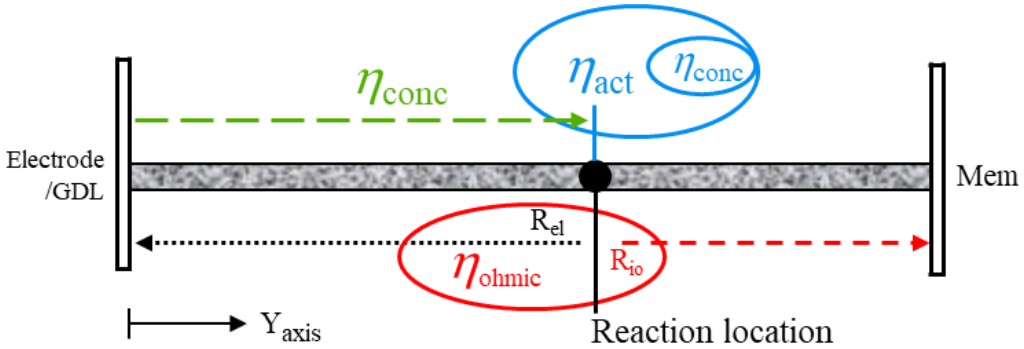

Fig. 6. Potential losses of HT-PEMFC at anodic CL

3.2.4 Discussions

The potential losses at inlet and along the gas channel of both anode and cathode

are examined at a temperature of 160 °C, as shown in Fig. 7. It can be seen that both η_{ohmic} and $\eta_{act+conc}$ increases with increasing current density at both anode and cathode (see Fig. 7(a & b)). However, the ratio of $\eta_{act+conc}/\eta_{ohmic}$ at anode has a slight increase while this value has a great decline from 94% to 58% at cathode. This is because the activation loss at the cathode dominates the cathode potential loss at a low current density while its relative importance is decreased at a higher current density, as the ohmic loss becomes the key loss at a higher current density (see Fig. 7(b)). At the anode side, $\eta_{act+conc}$ is relatively small compared with that at cathode. However, the percentage of $\eta_{act+conc}$ is slightly increased with increasing current density (see Fig. 7(a)). These results can explain the opposite trend between anode and cathode at inlet in Fig. 5(e & f).

The changes of each potential loss along the flow direction are examined in Fig. 7(c & d). The working condition is 160 °C and 0.4 V. It can be seen that η_{ohmic} at both anode and cathode slightly decrease along the flow direction. This can be attributed to the temperature increase along the flow direction, which leads to a higher ion conductivity and lower ohmic loss. However, the $\eta_{act+conc}$ at both anode and cathode increases along the flow channel as the lower reactant concentration increases the concentration overpotential and activation overpotential. Such change of η_{ohmic} and $\eta_{act+conc}$ leads to a bigger ratio of $\eta_{act+conc}/\eta_{ohmic}$ along the flow direction, which well explains the increase in ERT along the flow channel, as shown in Fig. 5(e & f). As for the results of Fig. 5(c & d), it becomes clear that the higher temperature decreases the ohmic loss and increases the ratio of $\eta_{act+conc}/\eta_{ohmic}$, leading to a higher ERT.

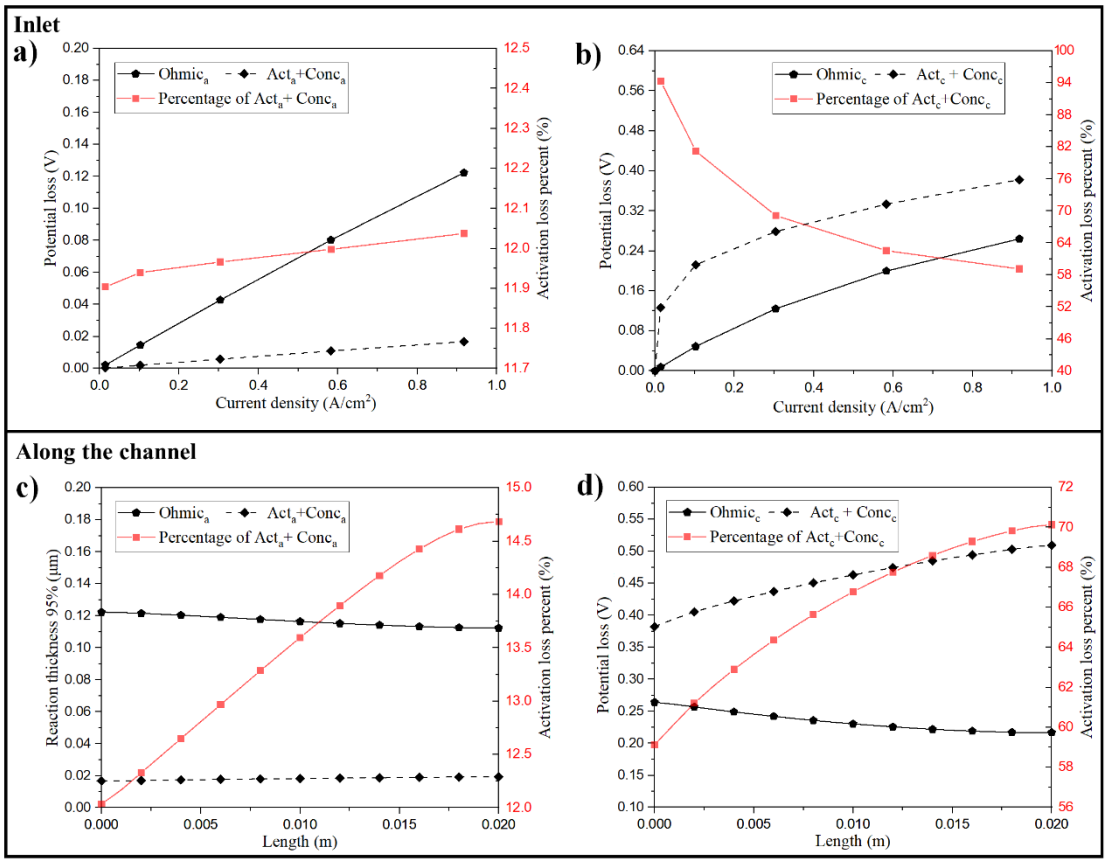

Fig. 7. Potential loss at inlet of anode a) and cathode b), Potential loss along the flow direction of anode c) and cathode d)

3.3 Effect of flow rate

Flow rate is one of the key controllable parameters that would significantly affect the cell performance. Normally the mass flow rate should be high enough to meet the requirements of electrical loading [46]. Otherwise, fuel cell may suffer from the reactants starvation which would greatly reduce the cell performance [47]. On the other hand, the flow rate should not be too high in order to save pumping power and to avoid excess thermal energy loss.

The effect of flow rate on ERT of both anode and cathode was shown in Fig. 8. The anode gas flow rate was in the range of 2-7 ml/min with a constant cathode flow rate of

29.11 ml/min calculated by equation (20) (see Fig. 8(a)). It is found that the effect of flow rate on ERT is negligible in the upstream. Away from the inlet, especially in the downstream of the anode, the flow rate effect becomes very significant and the ERT is substantially increased at a low flow rate. Due to the decreased concentrations of the reactants, the local equilibrium potential decreases along the gas channel, which in turn leads to decreasing local current density. Besides, such effect would be strengthened when a low flow rate is adopted. Therefore, the activation loss η_{act} and concentration loss η_{conc} are increased with decreasing flow rate. On the other hand, the temperature at the downstream is higher than that at the upstream, which leads to a decrease of ohmic loss η_{ohmic} along the flow direction. Thus, an increasing ERT of anodic CL was found with a decreasing flow rate. The fluctuation of anode ERT is due to the interpolation process of data points by the simulation software.

The cathodic ERT remains almost unchanged with different anode flow rate. Only a small increase of ERT can be found near the outlet. This can be attributed to the adequate supply of oxygen.

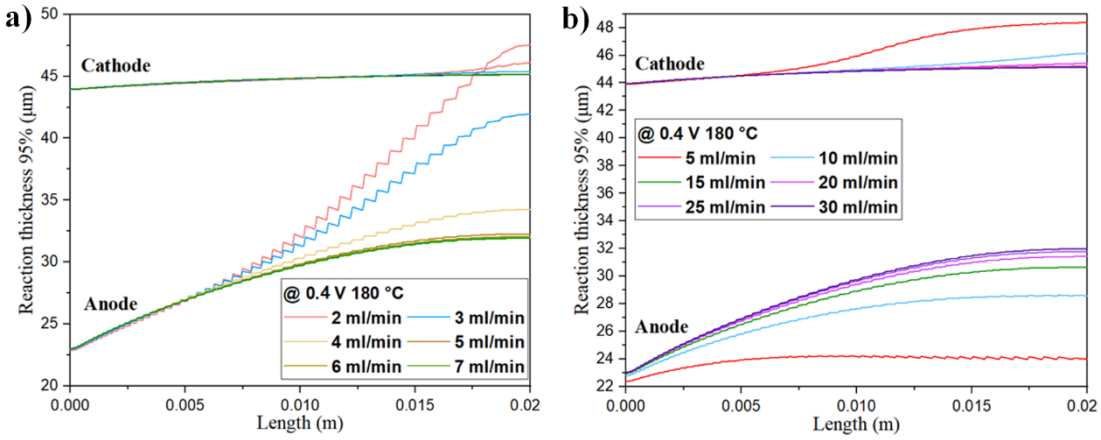

Fig. 8. Effective reaction thickness with different flow rate of a) anode and b) cathode

The cathode gas flow rate was in the range of 5-20 ml/min with a constant anode flow rate of 7.356 ml/min calculated by equation (21) (see Fig. 8(b)). The results show that both anodic and cathodic ERTs can be greatly affected by cathode flow rate. When a lower cathodic flow rate is adopted, cathodic ERT would increase a lot along the flow direction while a decrease of ERT can be observed at anode side. This opposite effect on ERT is another evidence of the result in Fig. 5(e & f) since low flow rate can lead to a low current density. Thus, it can be explained by the change of ratio of $\eta_{act+conc}/\eta_{ohmic}$ as well.

3.4 Effect of CL thickness

Various thicknesses are adopted in the previous work like 60-120 μm [48], 30-50 μm [49] and etc. Besides, the platinum coating accounts for a large proportion of the total cost of HT-PEMFC [21]. The cost of the CL is proportional to the thickness of CL, while the cost of the Pt-based CL contributes significantly to the total cost of HT-PEMFC [30]. On the other hand, the CL thickness also affects the electrochemical performance of fuel cell, as a too thin CL may not be able to provide the required reaction sites. Thus, the CL thickness must be carefully selected to achieve high performance with low cost.

In this section, different ERTs with different anodic and cathodic CL thicknesses were investigated. The effect of anodic CL thickness was examined ranging from 5 μm to 50 μm with cathodic CL thickness to be 50 μm as shown in Fig. 9(a & b). The working conditions are 160 °C and 0.6 V in consideration of the practical application. When a thinner anodic CL thickness is adopted, the anodic ERT remains almost

unchanged along the channel. The anodic ERT grows with the CL thickness. When the CL thickness is relatively thick, ERT increases slightly along the flow direction. The ERT of the cathode is almost unchanged with changing CL thickness of the anode. Our preliminary simulation results suggest that the ERT of cathode CL is almost independent of the anode CL thickness. To study the effect of CL thickness on the ERT, its value was varied from 5 μm to 100 μm with a constant anodic CL thickness of 50 μm. As shown in Fig. 9(c & d), cathodic CL thickness's effect on cathodic ERT is similar with the result of anodic CL thickness. However, anodic ERT is found to decrease more substantially with increase CL thickness of the cathode. This can be attributed to the increasing cathodic ohmic loss by the thicker cathodic CL thickness, which would reduce the cell performance.

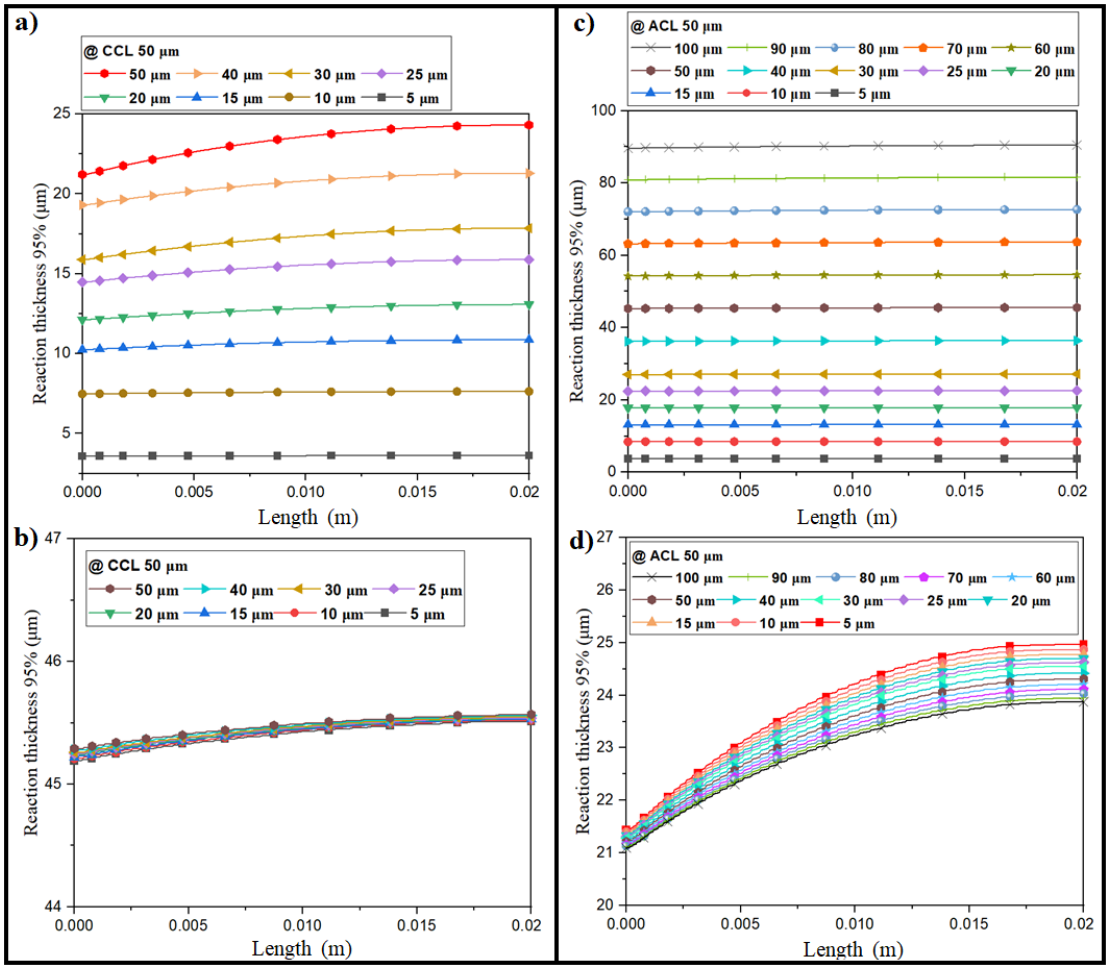

Fig. 9. Effective reaction thickness along the flow direction at a) anode and b) cathode with different anodic CL thicknesses and at c) cathode and d) anode with different cathodic CL thicknesses

To determine the appropriate CL thickness for practical application, the utilization rate is defined in this study as shown in Fig.10 (a). Take the anodic CL thickness of 25 μm in Fig. 9(a) as an example. The coordinate frame line can be regarded as a whole anodic CL. Thus, the area below the ERT curve along the flow direction represents 95% of the whole reaction amount. The utilization rate can be calculated as the effective reaction area divided by the total CL area, whose value is 60.96% under this circumstance. With different CL values, various utilization rate can be achieved (see

Fig. 10(b & c)). The current densities of all data points are added together to represent the cell performance with different parameters.

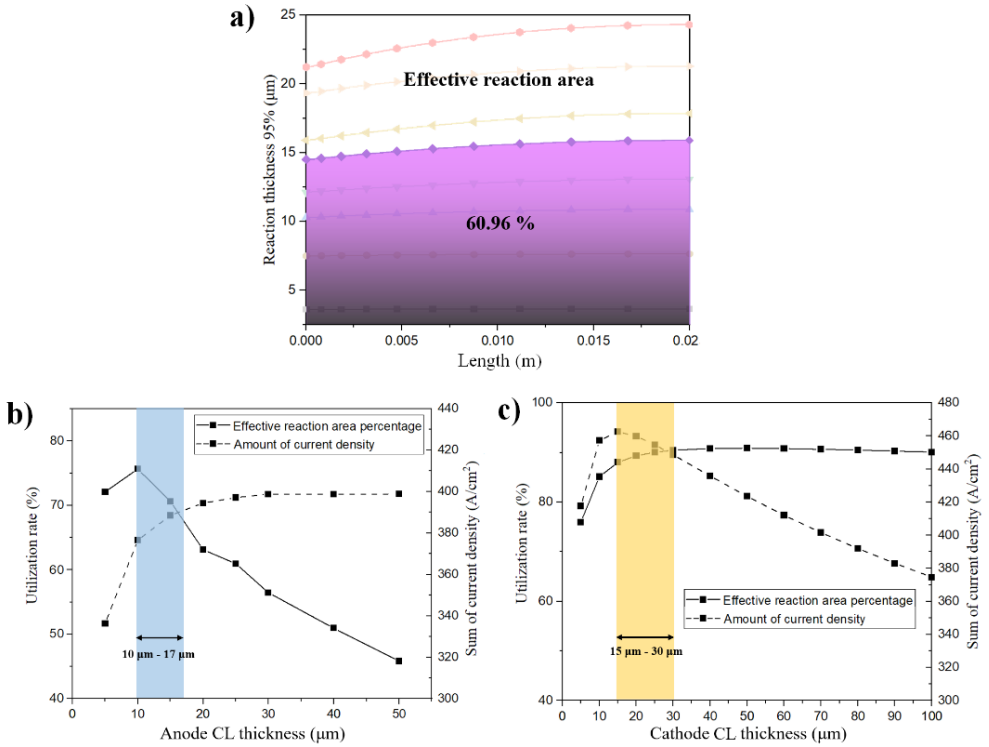

Fig. 10. a) schematic of utilization rate of the CL thickness, utilization rate and cell performance with different b) anodic CL thickness and c) cathodic CL thickness

In Fig. 10(b), the utilization rate of anodic CL increases when the CL thickness is increased from 5 μm to 10 μm and continuously decreases when the CL thickness is further increased from 10 μm to 50 μm. The peak value of the utilization rate is about 76%. However, in the range of 5-50 μm, the amount of reaction significantly increases with increasing CL thickness at first and then approaches to a constant value with a further increase in CL thickness. It means the reaction sites are insufficient when the CL thickness is small (e.g., less than 10 μm). Thus, increasing the CL thickness is beneficial to improve the fuel cell performance. However, when the reaction sites are sufficient, further increase in CL thickness (e.g., larger than 20 μm) will not further

improve the fuel cell performance. Therefore, the appropriate anodic CL thickness can be proposed in the range of 10-17 μm to achieve both high performance and low cost of CL. Apparently, this thickness range is much smaller than the commonly used 50 μm, which means the fuel cell cost can be reduced by reducing the anodic CL thickness from 50 μm to about 17 μm, without sacrificing the fuel cell performance.

As for the cathodic CL, its utilization rate is increased when CL thickness is increased from 5 μm to 40 μm and approaches to a constant value of about 90% when the CL thickness is further increased from 40 μm to 100 μm. In other words, the amount of reaction has an obvious growth when the cathodic CL thickness increases from 5-30 μm due to the same reason of increasing reaction sites. It can be revealed that the reaction sites would be sufficient when the cathodic CL thickness is small (e.g., less than 30 μm). However, when the reactions sites for cathodic ORR are sufficient, a decline of the cell performance can be observed with a further increase of cathodic CL thickness (e.g., larger than 15μm), which can be attributed to the increasing ionic and electronic resistance. Thus, the appropriate cathodic CL thickness can be proposed in the range of 15-30 μm taking into consideration of both cost and cell performance. Similar with the results of anodic CL thickness, the cathodic CL thickness can be reduced from 50 μm to about 30 μm, in which case the cost of catalyst can be reduced by 40% with a good cell performance.

4. Conclusion

In this work, a numerical non-isothermal 3D model was developed to investigate the ERT of both anode and cathode catalyst layer. Unlike previous studies on the

coupled transport and reaction processes in CL, the overpotential losses including the activation loss, concentration loss and ohmic loss are calculated respectively at two electrodes. What's more, the cost and cell performance are taken into consideration.

It is found that effects of working conditions on ERT of CL such as temperature, working voltage and flow rate can be explained by the ratio variation of $\eta_{act+conc}/\eta_{ohmic}$. A higher value of this ratio would lead to a larger ERT. Besides, the results show that the appropriate CL thicknesses for anode and cathode electrode are 10-17 μm and 15-30 μm, in which range the high utilization rate and good cell performance can be acquired. This finding is useful to identify CL thickness to achieve high performance with minimal CL cost.

It should be noted that the durability of the HT-PEMFC is not considered in the present study. In practices, the durability of HT-PEMFC is affected by various factors, such as carbon corrosion, loss of Pt catalyst etc. Interested readers may refer to the recent literature review articles on durability of fuel cells. When a thinner CL is adopted, the mechanical strength of CL might be reduced. Bolts are usually used for fuel cell assembly, which will cause compressive stress pressure on the fuel cell. Deformation of the GDL and the CL could happen under this stress, which may damage the microstructure of the CL and decrease the durability of the HT-PEMFC. In the subsequent studies, the durability of the HT-PEMFC should be studied by considering the mechanical stress of the cell.

Although this research is performed on HT-PEMFC. The method of determining the appropriate CL thickness can be widely applied to other kinds of fuel cells. Future

work should be conducted to experimentally realize the optimized CL design.

Acknowledgement

M. Ni thanks the funding support (Project Number: PolyU 152064/18E) from Research Grant Council, University Grants Committee, Hong Kong SAR. K.Q. ZHENG thanks the funding support (Project Number: 51806241) from National Natural Science Foundation of China. L.C. XIA thanks Mrs. Mengxiao Li (Chongqing University) for providing guidance from experimental view.

Reference

[1] Li H, Tang Y, Wang Z, Shi Z, Wu S, Song D, et al. A review of water flooding issues in the proton exchange membrane fuel cell. Journal of Power Sources. 2008;178:103-17.

[2] Jannelli E, Minutillo M, Perna A. Analyzing microcogeneration systems based on LT-PEMFC and HT-PEMFC by energy balances. Applied Energy. 2013;108:82-91.

[3] Rosli R, Sulong A, Daud W, Zulkifley M, Husaini T, Rosli M, et al. A review of high-temperature proton exchange membrane fuel cell (HT-PEMFC) system. International Journal of Hydrogen Energy. 2017;42:9293-314.

[4] Li Q, He R, Gao J-A, Jensen JO, Bjerrum NJ. The CO poisoning effect in PEMFCs operational at temperatures up to 200 C. Journal of the Electrochemical Society. 2003;150:A1599.

[5] Araya SS, Zhou F, Liso V, Sahlin SL, Vang JR, Thomas S, et al. A comprehensive review of PBI-based high temperature PEM fuel cells. International Journal of Hydrogen Energy. 2016;41:21310-44.

[6] Ribeirinha P, Abdollahzadeh M, Pereira A, Relvas F, Boaventura M, Mendes A. High temperature PEM fuel cell integrated with a cellular membrane methanol steam reformer: Experimental and modelling. Applied Energy. 2018;215:659-69.

[7] Fu X, Li T, Tang L, Deng X, Zhang R, Hu S, et al. Reticulated polyaniline nanowires as a cathode microporous layer for high-temperature PEMFCs. International Journal of Hydrogen Energy. 2021. 46(12): 8802-8809.

[8] Nanadegani FS, Lay EN, Sunden B. Computational analysis of the impact of a micro porous layer (MPL) on the characteristics of a high temperature PEMFC. Electrochimica Acta. 2020;333:135552.

[9] Xu X, Yang W, Zhuang X, Xu B. Experimental and numerical investigation on effects of cathode flow field configurations in an air-breathing high-temperature PEMFC. International Journal of Hydrogen Energy. 2019;44:25010-20.

[10] Wu H-W, Ho T-Y, Han Y-J. Parametric optimization of wall-mounted cuboid rows installed in interdigitated flow channel of HT-PEM fuel cells. Energy. 2020:119261.

[11] Cheng Y, Zhang J, Wu X, Tang C, Yang S-z, Su P, et al. A template-free method to synthesis high density iron single atoms anchored on carbon nanotubes for high temperature polymer electrolyte membrane fuel cells. Nano Energy.80:105534.
[12] Xiao T, Wang R, Chang Z, Fang Z, Zhu Z, Xu C. Electrolyte membranes for intermediate temperature proton exchange membrane fuel cell. Progress in Natural Science: Materials International. 2020, 30(6): 743-750.
[13] Eren EO, Özkan N, Devrim Y. Polybenzimidazole-modified carbon nanotubes as a support material for platinum-based high-temperature proton exchange membrane fuel cell electrocatalysts. International Journal of Hydrogen Energy. 2020.in press.
[14] Kannan A, Aili D, Cleemann LN, Li Q, Jensen JO. Three-layered electrolyte membranes with acid reservoir for prolonged lifetime of high-temperature polymer electrolyte membrane fuel cells. International Journal of Hydrogen Energy. 2020;45:1008-17.
[15] Schonvogel D, Rastedt M, Wagner P, Wark M, Dyck A. Impact of accelerated stress tests on high temperature PEMFC degradation. Fuel Cells. 2016;16:480-9.
[16] Rastedt M, Schonvogel D, Wagner P. Impact of Load Cycling at High Current Densities on the Degradation Behavior of Membrane-Electrode-Assemblies. ECS Transactions. 2014;64:741.
[17] Xu H, Song H, Xu C, Wu X, Yousefi N. Exergy analysis and optimization of a HT-PEMFC using developed Manta Ray Foraging Optimization Algorithm. International Journal of Hydrogen Energy. 2020;45:30932-41.
[18] Nazar K, Jaffery MH, Shakir I, Nazar A, Raza R. Design of 1kW high temperature PEM fuel cell system and performance analysis under different operating conditions. Current Applied Physics. 2020. in press.
[19] Lu X, Ren J, Guo L, Wang P, Yousefi N. Improved grass fibrous root algorithm for exergy optimization of a high-temperature PEMFC. Energy Reports. 2020;6:1328-37.
[20] Ghosh P, Mandal S, Majumdar S, Sarkar A, Ganguly S, Kargupta K. Enhanced power generation, faster transient response and longer durability of HT-PEMFC using composite polybenzimidazole electrolyte membrane with optimum rGO loading. International Journal of Hydrogen Energy. 2020, 45(33): 16708-16723.
[21] Wei M, Lipman T, Mayyas A, Chien J, Chan SH, Gosselin D, et al. A total cost of ownership model for low temperature PEM fuel cells in combined heat and power and backup power applications. Lawrence Berkeley National Lab.(LBNL), Berkeley, CA (United States); 2014.
[22] Scofield ME, Liu H, Wong SS. A concise guide to sustainable PEMFCs: recent advances in improving both oxygen reduction catalysts and proton exchange membranes. Chemical Society Reviews. 2015;44:5836-60.
[23] Rath R, Kumar P, Unnikrishnan L, Mohanty S, Nayak SK. Current Scenario of Poly (2, 5-Benzimidazole)(ABPBI) as Prospective PEM for Application in HT-PEMFC. Polymer Reviews. 2020;60:267-317.
[24] Wang K, Chen H, Zhang X, Tong Y, Song S, Tsiakaras P, et al. Iron oxide@ graphitic carbon core-shell nanoparticles embedded in ordered mesoporous N-doped carbon matrix as an efficient cathode catalyst for PEMFC. Applied Catalysis B: Environmental. 2020;264:118468.
[25] Bevilacqua N, Asset T, Schmid M, Markötter H, Manke I, Atanassov P, et al. Impact of catalyst layer morphology on the operation of high temperature PEM fuel cells. Journal of Power Sources Advances.7:100042.
[26] Zagoraiou E, Paloukis F, Neophytides SG, Daletou MK. The electrochemical interface of the

cathode in high temperature PEM fuel cells. Electrochimica Acta. 2020;356:136778.
[27] Martin S, Li Q, Jensen JO. Lowering the platinum loading of high temperature polymer electrolyte membrane fuel cells with acid doped polybenzimidazole membranes. Journal of Power Sources. 2015;293:51-6.
[28] Martin S, Jensen J, Li Q, Garcia-Ybarra P, Castillo J. Feasibility of ultra-low Pt loading electrodes for high temperature proton exchange membrane fuel cells based in phosphoric acid-doped membrane. International Journal of Hydrogen Energy. 2019;44:28273-82.
[29] Siddique N, Liu F. Process based reconstruction and simulation of a three-dimensional fuel cell catalyst layer. Electrochimica Acta. 2010;55:5357-66.
[30] You L, Liu H. A parametric study of the cathode catalyst layer of PEM fuel cells using a pseudo-homogeneous model. International Journal of Hydrogen Energy. 2001;26:991-9.
[31] Siegel N, Ellis M, Nelson D, Von Spakovsky M. Single domain PEMFC model based on agglomerate catalyst geometry. Journal of Power Sources. 2003;115:81-9.
[32] Scott K, Pilditch S, Mamlouk M. Modelling and experimental validation of a high temperature polymer electrolyte fuel cell. Journal of Applied Electrochemistry. 2007;37:1245-59.
[33] Sasiwimonrit K, Chang W-C. To improve the high temperature polymer electrolyte membrane fuel cells performance by altering the properties of catalyst layer. International Journal of Hydrogen Energy. 2020, 45(28): 14491-14499.
[34] Kamarajugadda S, Mazumder S. Numerical investigation of the effect of cathode catalyst layer structure and composition on polymer electrolyte membrane fuel cell performance. Journal of Power Sources. 2008;183:629-42.
[35] Xia L, Zhang C, Hu M, Jiang S, Chin CS, Gao Z, et al. Investigation of parameter effects on the performance of high-temperature PEM fuel cell. International Journal of Hydrogen Energy. 2018;43:23441-9.
[36] Haider R, Wen Y, Ma Z-F, Wilkinson DP, Zhang L, Yuan X, et al. High temperature proton exchange membrane fuel cells: progress in advanced materials and key technologies. Chemical Society Reviews. 2021, 50: 1138-1187.
[37] Lin H-L, Yu TL, Chang W-K, Cheng C-P, Hu C-R, Jung G-B. Preparation of a low proton resistance PBI/PTFE composite membrane. Journal of power sources. 2007;164:481-7.
[38] Lee MR, Lee HY, Yim SD, Kim CS, Shul YG, Kucernak A, et al. Effects of ionomer carbon ratio and ionomer dispersity on the performance and durability of MEAs. Fuel Cells. 2018;18:129-36.
[39] Li S, Sundén B. Three-dimensional modeling and investigation of high temperature proton exchange membrane fuel cells with metal foams as flow distributor. International Journal of Hydrogen Energy. 2017;42:27323-33.
[40] TEK E. Gas Diffusion Electrodes and Catalyst Materials. 1995 Catalogue. 1995.
[41] Coker AK. Appendix C: Physical properties of liquids and gases. Ludwig's Applied Process Design for Chemical and Petrochemical Plants. 2007;1:827-62.
[42] Chase Jr MW. NIST-JANAF thermochemical tables. J Phys Chem Ref Data, Monograph. 1998;9.
[43] Ubong E, Shi Z, Wang X. Three-dimensional modeling and experimental study of a high temperature PBI-based PEM fuel cell. Journal of The Electrochemical Society. 2009;156:B1276.
[44] Mench MM. Fuel cell engines: John Wiley & Sons; 2008.
[45] Chen DF, Zeng QC, He HH, Wei L, Yu ZD. Equivalent circuit model for the electrochemical reaction process within the solid oxide fuel cell composite electrode. Advanced Materials Research: Trans Tech Publ; 2013. p. 266-72.

[46] Arsalis A, Nielsen MP, Kær SK. Modeling and parametric study of a 1 kWe HT-PEMFC-based residential micro-CHP system. International Journal of Hydrogen Energy. 2011;36:5010-20.
[47] Giotakos P, Neophytides S. Physical modeling of the electrochemical impedance spectra for the O2 reduction reaction in HTPEM fuel cells' cathodic electrochemical interface. Electrochimica Acta. 2018;292:285-91.
[48] Liu S, Rahim Y, Wippermann K, Janßen H, Lehnert W, Stolten D. Study of Cathode Catalyst Layer Parameters for HT-PEMFC Using Electrochemical Impedance Spectroscopy. ECS Transactions. 2017;80:27.
[49] Herdem MS, Mundhwa M, Farhad S, Hamdullahpur F. Catalyst layer design and arrangement to improve the performance of a microchannel methanol steam reformer. Energy Conversion and Management. 2019;180:149-61.